Biochimica et Biophysica Acta 1852 (2015) 1477–1489

Contents lists available at ScienceDirect

Biochimica et Biophysica Acta

journal homepage: www.elsevier.com/locate/bbadis

miR-155-dependent regulation of mammalian sterile 20-like kinase 2 (MST2) coordinates inflammation, oxidative stress and proliferation in vascular smooth muscle cells

Zhan Yang, Bin Zheng, Yu Zhang, Ming He, Xin-hua Zhang, Dong Ma, Ruo-nan Zhang, Xiao-li Wu, Jin-kun Wen *

Department of Biochemistry and Molecular Biology, The Key Laboratory of Neural and Vascular Biology, China Administration of Education, Hebei Medical University, Shijiazhuang, China

ARTICLE INFO

Article history:
Received 6 January 2015
Received in revised form 29 March 2015
Accepted 8 April 2015
Available online 17 April 2015

Keywords:
VSMC
Proliferation
miR-155
MST2
Inflammation
Oxidative stress

ABSTRACT

In response to vascular injury, inflammation, oxidative stress, and cell proliferation often occur simultaneously in vascular tissues. We previously observed that microRNA-155 (miR-155), which is implicated in proliferation and inflammation is involved in neointimal hyperplasia; however, the molecular mechanisms by which it regulates these processes remain largely unknown. In this study, we observed that vascular smooth muscle cell (VSMC) proliferation and neointimal formation in wire-injured femoral arteries were reduced by the loss of miR-155 and increased by the gain of miR-155. The proliferative effect of miR-155 was also observed in cultured VSMCs. Notably, expression of the miR-155-target protein mammalian sterile 20-like kinase 2 (MST2) was increased in the injured arteries of miR-155$^{-/-}$ mice. miR-155 directly repressed MST2 and thus activated the extracellular signal-regulated kinase (ERK) pathway by promoting an interaction between RAF proto-oncogene serine/threonine-protein kinase (Raf-1) and mitogen-activated protein kinase kinase (MEK) and stimulating inflammatory and oxidative stress responses; together, these effects lead to VSMC proliferation and vascular remodeling. Our data reveal that MST2 mediates miR-155-promoted inflammatory and oxidative stress responses by altering the interaction of MEK with Raf-1 and MST2 in response to vascular injury. Therefore, suppression of endogenous miR-155 might be a novel therapeutic strategy for vascular injury and remodeling.

1. Introduction

In response to vascular injury, vascular smooth muscle cells (VSMCs) undergo a series of characteristic changes including phenotypic modulation, abnormal proliferation, migration, matrix synthesis, and inflammation [1]; these events are crucial for the development and progression of vascular remodeling diseases such as atherosclerosis, hypertension, and restenosis after angioplasty. VSMCs are the principal effector cells in this process; therefore VSMCs coordinate and synchronize extremely complex inflammatory, proliferative, differentiation and oxidative stress programs [2,3]. Although a few pathophysiological mechanisms associated with VSMC proliferation, inflammation and oxidative stress are known, the molecular mechanisms by which the VSMC responses to injury are coordinated remain unclear.

MicroRNAs (miRNAs) regulate gene expression at the post-transcriptional level by promoting mRNA degradation or by inhibiting translation and play a critical role in vascular inflammation and remodeling [4]. Several miRNAs such as miR-21, miR-126, miR-133, miR-143/145, miR-146a, and miR-221/222 have been implicated in vascular inflammation and remodeling [5]. For example, miR-133 inhibits VSMC proliferation by targeting transcription factor Sp1 [6], and miR-221/222 promotes VSMC proliferation by targeting p27 and p57 [7]. miR-143/145 are molecular keys that switch the VSMC phenotype [8]. miR-126 inhibits vascular cell adhesion molecule 1 (VCAM-1) expression and reduces leukocyte adherence to endothelial cells [9]. miR-155 is a target of several inflammatory mediators. Recently, we found that miR-155 is involved in neointimal formation in carotid arteries after angioplasty [10]. miR-155 is a pleiotropic regulator of inflammation-related diseases and is critical for various physiological and pathological processes including inflammation, differentiation, carcinogenesis, oxidative stress, and cardiovascular remodeling [11,12]. However, the role of miR-155 in coordinating inflammation, oxidative stress and vascular remodeling has not been elucidated.

The mammalian sterile 20-like kinase 2 (MST2), also called Ser/Thr kinase 3 (STK3), and its close homolog MST1 (STK4) are members of the germinal center kinase group II family which are mitogen-activated protein kinase (MAPK)-related kinases [13]. As a core component of the Hippo pathway in mammalian cells, MST2 regulates cell proliferation, growth and apoptosis [14]. Proteomic analysis of RAF proto-oncogene

* Corresponding author at: Department of Biochemistry and Molecular Biology, Key Laboratory of Neural and Vascular Biology, Ministry of Education, Hebei Medical University, No. 361 Zhongshan East Road, Shijiazhuang 050017, China. Tel.: +86 31186265563; fax: +86 31186266180.
E-mail address: wjk@hebmu.edu.cn (J. Wen).

http://dx.doi.org/10.1016/j.bbadis.2015.04.012
0925-4439/

serine/threonine-protein kinase (Raf-1) signaling complexes revealed that Raf-1 interacts with MST2 and counteracts apoptosis by suppressing the activation of MST2 [15]. MST2 binds to Raf-1 at two distinct sites that partially overlap with the mitogen-activated protein kinase kinase (MEK)-binding domain on Raf-1 [16], suggesting that MST2 competes with MEK to bind to Raf-1 and affects the MAPK signaling cascade. Furthermore, the interaction between MST2 and Raf-1 regulates the ERK1/2 pathway and inhibits the pro-apoptotic activation of MST2 [15,17]. Although MST1/2 activates Ser/Thr protein kinases and regulates the Raf-1/ERK pathway activity, the role of MST2 in regulation of inflammation and oxidative stress in VSMCs has not been studied.

In this study, we investigated whether and how MST2 mediates miR-155-promoted inflammation and oxidative stress, which lead to VSMC proliferation and vascular remodeling, through integrating inflammatory and oxidative stress signaling.

2. Materials and methods

2.1. Animal models

All animal studies were approved by the Institutional Animal Care and Use Committee of Hebei Medical University (approval ID: HebMU 20080026) and all efforts were made to minimize suffering. Eight- to 12-week-old male wild-type C57BL/6 mice and miR-155$^{-/-}$ mice (Jackson Laboratory, Bar Harbor, ME) were anesthetized with 1.5% isoflurane. To reproducibly induce vascular remodeling, we performed femoral artery wire injury as previously described [18]. Briefly, we carefully separated the left femoral artery and the accompanying femoral nerve under anesthesia. A small branch of the femoral artery was isolated under the muscles. The femoral artery and the small branch were looped with 6–0 silk sutures to temporarily stop blood flow during the procedure. A spring wire (0.38-mm diameter, Cook Inc., Bloomington, IN) was inserted into the femoral artery more than 5 mm and moved in and out twice. The wire was then removed, and blood flow in the femoral artery and branch was restored by releasing the sutures, and the skin incision was closed with a 5–0 silk suture. The other femoral artery was sham-operated and served as a control.

For the miR-155-overexpression model, femoral artery wire injury was performed as described above. Immediately after injury, the femoral artery was cannulated, and the biclamped segment was incubated with 20 μl of adenovirus (1×10^{10} pfu/ml) encoding miR-155 or GFP for 15 min. After 14 days, all animals were anesthetized and perfused with cold 0.9% NaCl, and the tissues were harvested for analysis of RNA, morphology, and histology.

2.2. Morphometry and histology

Mice were euthanized, perfused and then fixed with 4% paraformaldehyde in 0.9% NaCl for 3 min through the left ventricle under physiological pressure. The femoral arteries were harvested, fixed with formalin and embedded in paraffin. Ten consecutive 5-μm-thick sections were prepared for hematoxylin and eosin staining; the sections were prepared at intervals of 550 μm. Images were acquired using a Leica microscope (Leica DM6000B, Switzerland) and digitized with LAS V.4.4 (Leica). Morphometric analysis of the neointimal area and measurement of the intima/media (I/M) ratio were performed in a blind manner.

2.3. Immunofluorescence staining

Immunofluorescence staining was performed with 5 μm paraffin cross-sections from the femoral artery. After deparaffinized with xylene and rehydrated, the slides were pre-incubated with 10% normal goat serum (710027, KPL, USA) and then incubated with primary antibodies anti-SM22α (ab14106, Abcam), anti-MAC2 (60207-1, Proteintech), anti-MST2 (ab52641, Abcam). Secondary antibodies were fluorescein-labeled antibody to rabbit IgG (021516, KPL, USA) and rhodamine-labeled antibody to mouse IgG (031806, KPL, USA), or fluorescein-labeled antibody to mouse IgG (021815, KPL, USA), rhodamine-labeled antibody to rabbit IgG (031506, KPL, USA). In each experiment, DAPI (157574, MB biomedical) was used for nuclear counter staining. Images were captured by confocal microscopy (DM6000 CFS, Leica) and processed by LAS AF software.

2.4. In situ hybridization

Paraffin cross-sections (5-μm thick) from femoral arteries were deparaffinized and rehydrated for *in situ hybridization* according to user manual of miRCURY LNATM microRNA ISH Optimization Kit (Exiqon). Hybridization was performed using fluorescence-labeled miR-155 probes (50 nM) in hybridization buffer (Exiqon) by incubation at 55 °C for 1 h in a thermoblock (Labnet). After stringent washing with SSC buffer, nonspecific binding sites were blocked with 10% normal goat serum (710027, KPL, USA). The sections were then incubated for 1 h at 37 °C with anti-SM22α primary antibody (ab14106, Abcam) diluted 1:50 in PBS. After washing with PBS, the sections were incubated with a rhodamine-labeled secondary antibody (031506, KPL, USA) at 37 °C for 30 min. Images were acquired using a Leica microscope (Leica DM6000B, Switzerland) and digitized with a software of LAS V.4.4 (Leica).

2.5. Isolation of mRNA and real time PCR

Total RNA was extracted from femoral arteries, which were homogenized with gentle MACSTM Dissociator (Miltenyi Biotec), and cultured VSMCs using the Trizol (Invitrogen^{TM}) according to the manufacturer's instructions. The quality of the RNA was determined using a Biospectrometer (Eppendorf). For microRNA: reverse transcription and qRT-PCR was performed using the Taqman microRNA Reverse Transcription kit and TaqMan Universal Master MixII (Applied Biosystems) with specific primers for mmu-miR-155 (Assay ID: 001806) and internal control RNU6b (U6) (Assay ID: 001093) according to the manufacturer's protocol. For large mRNA: cDNA was synthesized using an M-MLV First Strand Kit (Life Technologies). qRT-PCR of mRNAs was performed using Platinum SYBR Green qPCR Super Mix UDG Kit (Invitrogen), and real-time PCR experiments were carried on a ABI 7500 FAST system (Life Technologies). Relative amount of transcripts was normalized with GAPDH and calculated using the $2^{-\Delta\Delta Ct}$ formula as previously described [19]. Supplementary Table I summarizes the primer sequences.

2.6. Cell culture, siRNA transfection and plasmid constructs

Vascular smooth muscle cells were isolated from the thoracic aorta of male Sprague–Dawley rats (60–80 g) as previously described [19] and cultured in Dulbecco's modified Eagle's medium (DMEM, Gibco Life Technologies, Rockville, MD) containing 10% fetal calf serum (ABGENT), 100 units/ml of penicillin, and 100 μg/ml of streptomycin under 5% CO_2 atmosphere at 37 °C. VSMCs from passages 3 to 5 were used in experiments. 293A cells were maintained in high-glucose Dulbecco's modified Eagle's medium (DMEM, Gibco Life Technologies, Rockville, MD) supplemented with 10% FCS. All cells were transfected using Lipofectamine 2000 (Invitrogen) according to the manufacturer's protocol. Small interfering RNAs (siRNAs) against the rat MST2 sequence (accession number Genbank: NM_031735.1) were designed and synthesized by Sigma. The siRNA sequences used in these studies were as follows: MST2 siRNA#1: 5′-GGG UCC GUU UCA GAC AUA Att-3′; 5′-UUA UGU CUG AAA CGG AC CCtt-3′; MST2 siRNA#2: 5′-CGA GGU AAU UCA AGA AAU Att-3′; UAU UUC UUG AAU UAC CUC Gtt-3′; siControl: 5′-UUC UCC GAA CGU GUC ACG UTT-3′; 5′-ACG UGA CAC GUU CGG AGA ATT-3′. Twenty hours after transfection, the VSMCs were treated with 10% FCS. The cells were then harvested and lysed

for Western blotting analysis and coimmunoprecipitation assays. pCMV-Flag-MST2-MAT plasmid as a gift from Dr. YUAN (Chinese Academy of Sciences, Beijing). Genes 3′UTR contain miR-155 target site or its mutant sequences (Supplemental Table II) were inserted into pmir-GLO Dual-Luciferase miRNA Target Expression Vector (Promega).

2.7. Cell counting

The cell number was determined using a Countess™ Automated Cell Counter (Invitrogen) as previously described [20] after transfection with Ad-miR-155 or Ad-GFP, or anti-miR-155, and or anti-miR-ctl in different periods. Untreated cells were used for the baseline count; each sample was counted three times, and the average value from triplicate experiments was measured.

2.8. MTS assay

After appropriate treatment, viability of the VSMCs cultured in 96-well plates was measured using the MTS assay, as previously described [21]. In brief, the medium of cultured VSMCs was replaced with 100 μl serum-free DMEM containing 10 μl of CellTiter 96 AQueous One Solution (Promega, G3582). Control reactions were performed in triplicate using the same reagents without cells. The plates were then incubated at 37 °C for 4 h. Then, 60 μl of medium from each well was transferred to a new 96-well plate, and the absorbance was at 490 nm was measured using a Multiskan spectrum (Thermo). The control absorbance at 490 nm was subtracted from the average absorbance to obtain the corrected absorbance.

2.9. Western blot analysis

Proteins from femoral artery were homogenized and cultured VSMCs were prepared with lysis buffer (1% Triton X-100, 150 mM NaCl, 10 mM Tris–HCl, pH 7.4, 1 mM EDTA, 1 mM EGTA, pH 8.0, 0.2 mM Na_3VO_4, 0.2 mM phenylmethylsulfonyl fluoride, and 0.5% NP-40). Equal amounts of protein were separated on 10% SDS-PAGE, and electrotransferred to a PVDF membrane (Millipore). Membranes were blocked with 5% milk in TTBS for 2 h at room temperature and incubated primary antibodies overnight at 4 °C. Antibodies that were used are as follow: anti-SM22α (1:1000, sc-50466), anti-PCNA (1:1000, sc-56), or anti-β-actin (1:1000, sc-47778), anti-ERK1/2 (1:1000, sc-93), anti-phospho-ERK1/2 (Thr202/Tyr204) (1:500, sc-81492), anti-Akt (1:1000, sc-4060), anti-phospho-Akt (1:1000, sc-2985R), anti-Raf-1 (1:500, sc-7267), anti-phospho-Raf-1 (Ser338/Tyr341) (1:500, sc-28005R) were purchased from Santa Cruz Biotechnology; anti-JNK (1:500, #9252), anti-phospho-JNK (Tyr183/185) (1:400, #4668), anti-p38 MAPK (1:500, #9212), anti-phospho-p38 MAPK (Thr180/Tyr182) (1:400, #4511), anti-MEK1/2 (1:500, #9126) and anti-phospho-MEK1/2 (Ser217/221) (1:400, #9154), anti-caspase-3 (1:1000, #9662) were from Cell Signaling Technology; anti-MST2 (1:1000, ab52641) from Abcam Biotechnology; anti-NF-κB p65 (1:500, NBP1-96139) from NOVUS Biologicals; anti-phospho-NF-κB (Ser536) (1:400, AF2006) from Affinity Biotech; anti-$p47^{phox}$ (1:500, B1171), anti-phospho-$p47^{phox}$ (Ser370) (1:400, BS4852) from Bioworld Technology. Membranes were then incubated with the HRP-conjugated secondary antibody (1:5000, Rockland) for 1 h at room temperature. The blots were treated with the Immobilon™ Western (Millipore), and detected by ECL (enhanced chemiluminescence) Fuazon Fx (Vilber Lourmat). Images were captured and processed by FusionCapt Advance Fx5 software (Vilber Lourmat). All experiments were replicated three times.

2.10. Target prediction

Potential target genes of miR-155 were identified with following miRNA target prediction algorithms: miRanda (www.microrna.org) and RNAhybrid (http://bibiserv.techfak.uni-bielefeld.de/rnahybrid/submission.html) [22,23].

2.11. Luciferase assays

293A cells were transfected with a miR-155 mimic (30 nM, Ambion Pre-miR miRNA Precursor; Life Technologies), NC oligonucleotides (30 nM), or anti-miR-155 (30 nM, miRCURY LNA Inhibitor; Exiqon) combined with 100 ng of luciferase reporter or an empty vector. Luciferase activity was measured using a Dual-Glo Luciferase Assay System (Promega, Madison, WI) with a Flash and Glow (LB955, Berthold Technologies) reader 24 h after transfection. The specific target activity was expressed as the relative activity ratio of firefly luciferase to Renilla luciferase.

2.12. Co-immunoprecipitation assay

Co-immunoprecipitation was performed as described previously [24]. In brief, proteins from VSMCs were first pre-cleared with 30 μl of protein A-agarose (50% *v*/*v*). The supernatants were immunoprecipitated with 3 μg Raf-1 antibodies for 1 h at 4 °C and then incubated with protein A-agarose overnight at 4 °C. Protein A–agarose–antigen–antibody complexes were collected by centrifugation at 12,000 rpm for 2 min at 4 °C. The pellets were washed four times with 600 μl of IPH buffer (50 mM Tris–HCl, pH 8.0, 150 mM NaCl, 5 mM EDTA, 0.5% NP-40, and 0.1 mM phenylmethylsulfonyl fluoride) for 20 min at 4 °C. The bound proteins were resolved using SDS-PAGE followed by Western blotting using anti-MST2, anti-MEK and anti-Raf-1 antibodies.

2.13. Statistics

All of the data are presented as the means ± S.E.M. Differences between two groups were assessed using analysis of variance followed by a Student's *t*-test. A value of $P < 0.05$ was considered statistically significant.

3. Results

3.1. Loss and gain of miR-155 significantly decrease and increase neointimal formation in wire-injured vessels, respectively

To examine whether miR-155 is a key mediator in vascular remodeling, C57BL/6 mice were subjected to femoral artery wire denudation injury and examined after 14 days. Notably, the injured vessels in miR-$155^{-/-}$ mice showed decreased neointimal hyperplasia, intima-to-media ratio and stenosis compared with WT mice (Fig. 1A, B). Next, we examined miR-155 expression levels in injured femoral arteries of WT and miR-$155^{-/-}$ mice. Quantitative real-time (qRT)-PCR analysis revealed that miR-155 expression was elevated by 3.5-fold in the injured arteries of WT mice compared to uninjured arteries and was barely detectable in miR-$155^{-/-}$ mice (Fig. 1C). The U6 small nuclear RNA, as an internal control, was relatively unchanged in various groups of mice (Supplementary Fig. 1A). In contrast, we overexpressed miR-155 using adenovirus (Ad)-mediated gene transfer; Ad-miR-155 was administered intraluminally after wire-induced injury [25]. qRT-PCR analysis revealed increased miR-155 expression in injured vessels 14 days after Ad-miR-155 infection (Supplementary Fig. 2A). As expected, miR-155 overexpression significantly increased neointimal formation, the intima/media ratio, and stenosis (Supplementary Fig. 2B, C).

To further confirm the role of miR-155 in vascular injury, wire-injured femoral arteries were treated locally with an agomir or antagomir of miR-155 to up-regulate or down-regulate miR-155, respectively. The results showed that treatment with the miR-155 agomir increased neointimal hyperplasia, intima-to-media ratio and stenosis compared with the control agomir. Conversely, miR-155 antagomir

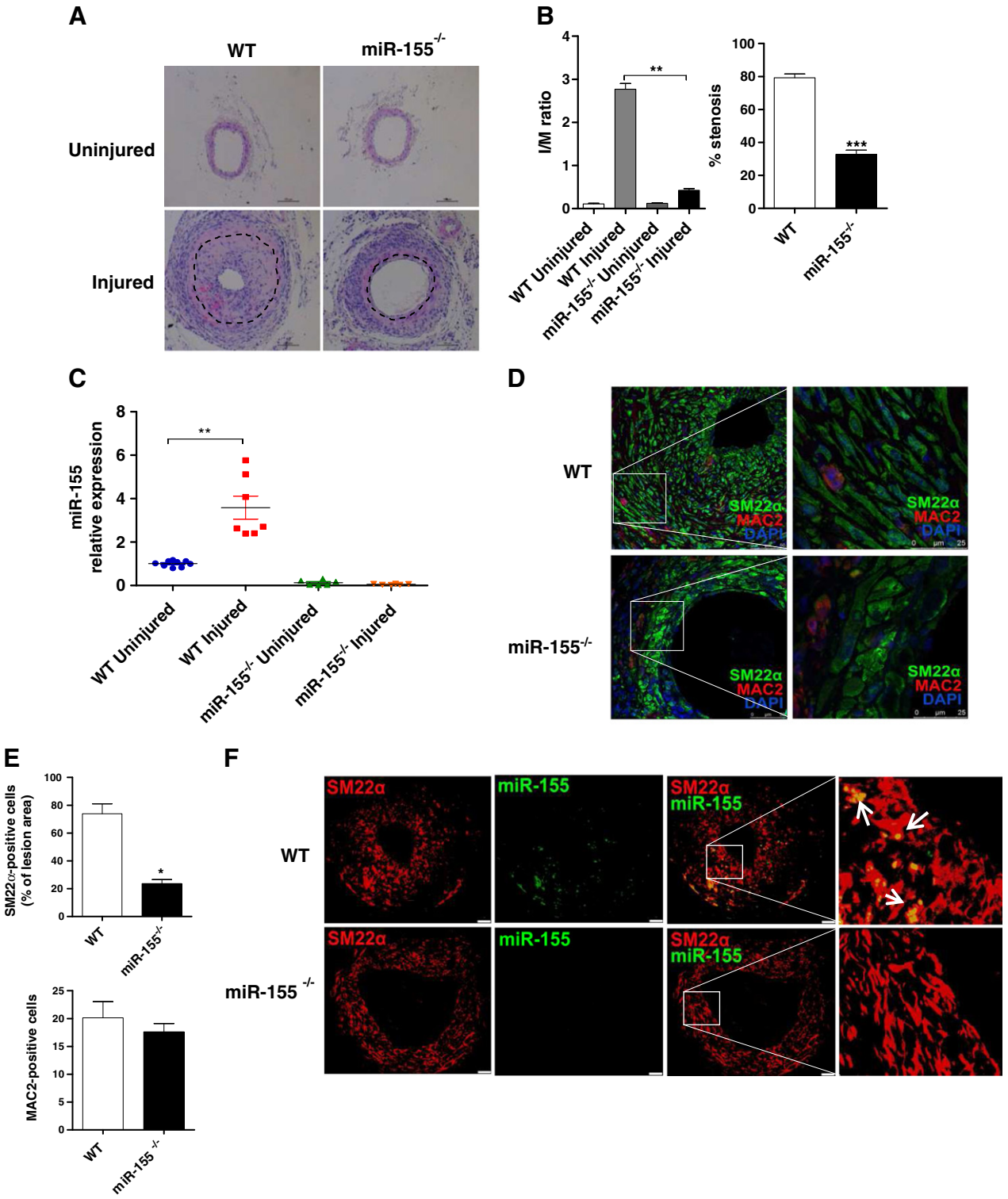

Fig. 1. Role of miR-155 in neointimal formation induced by wire injury in the femoral artery. A, Representative hematoxylin and eosin staining of cross sections from uninjured and wire-injured arteries; n = 9 for C57BL/6 (WT) mice; n = 7 for miR-155 knockout (miR-155$^{-/-}$) mice. Scale bar = 100 μm. B, The intima to media (I/M) ratio and stenosis. **P < 0.01 vs. WT injured; ***P < 0.001 vs. WT. C, qRT-PCR analysis of miR-155 expression. **P < 0.01 vs. WT uninjured n = 3. D, Immunofluorescence staining using specific anti-MAC2 and anti-SM22α antibodies. Scale bars = 50 μm. E, Analysis of SM22α-positive and MAC2-positive cells in the lesion area determined by immunofluorescence. *P < 0.05 vs. WT. F, In situ hybridization of miR-155 (green) combined with VSMC-specific SM22α staining (red) in the injured arteries of WT and miR-155$^{-/-}$ mice 14 days after injury. Arrows indicate miR-155-positive VSMCs. Scale bars = 32 μm.

decreased neointimal formation, the intima/media ratio, and stenosis compared with control antagomir (Supplementary Fig. 3A, B). These results suggest that miR-155 plays a vital role in neointimal formation induced by vascular endothelial injury.

Because VSMC proliferation and macrophage infiltration underlie the pathogenesis of neointimal formation [10], we examined the VSMC and macrophage contents in injured vessels. As shown in Fig. 1D and E, 14 days after injury, SM22α-positive cells comprised

73.9% of the lesion area within the neointima in WT mice but only 23.7% of the lesion area in miR-155$^{-/-}$ mice. However, the macrophage numbers in the lesion area (MAC2-positive cells) were not significantly different in WT and miR-155$^{-/-}$ mice. These observations suggest that VSMCs are likely the primary cellular source of miR-155 in injured vessels. To test this hypothesis, we performed in situ hybridization of miR-155 probe combined with SM22α immunostaining and observed that miR-155 was expressed mainly in the VSMCs but not the macrophages of the neointima (Fig. F). Together, these results indicate that miR-155 mediates VSMC proliferation, leading to neointimal formation after wire-induced vascular injury.

3.2. miR-155 promotes VSMC proliferation

To examine the role of miR-155 in VSMC proliferation, we used qRT-PCR to examine miR-155 expression in quiescent and proliferative VSMCs. The miR-155 expression level was significantly higher in PDGF-BB-stimulated VSMCs compared to serum-starved quiescent VSMCs (Fig. 2A). The U6 small nuclear RNA was relatively unchanged upon PDGF stimulation (Supplementary Fig. 1B). To elucidate whether miR-155 promotes VSMC proliferation, VSMCs cultured in 2% serum were transfected with anti-miR-155 or anti-miR-ctl and then treated with PDGF-BB. Western blotting analysis revealed that transfection with anti-miR-155 but not anti-miR-ctl inhibited PDGF-BB-induced

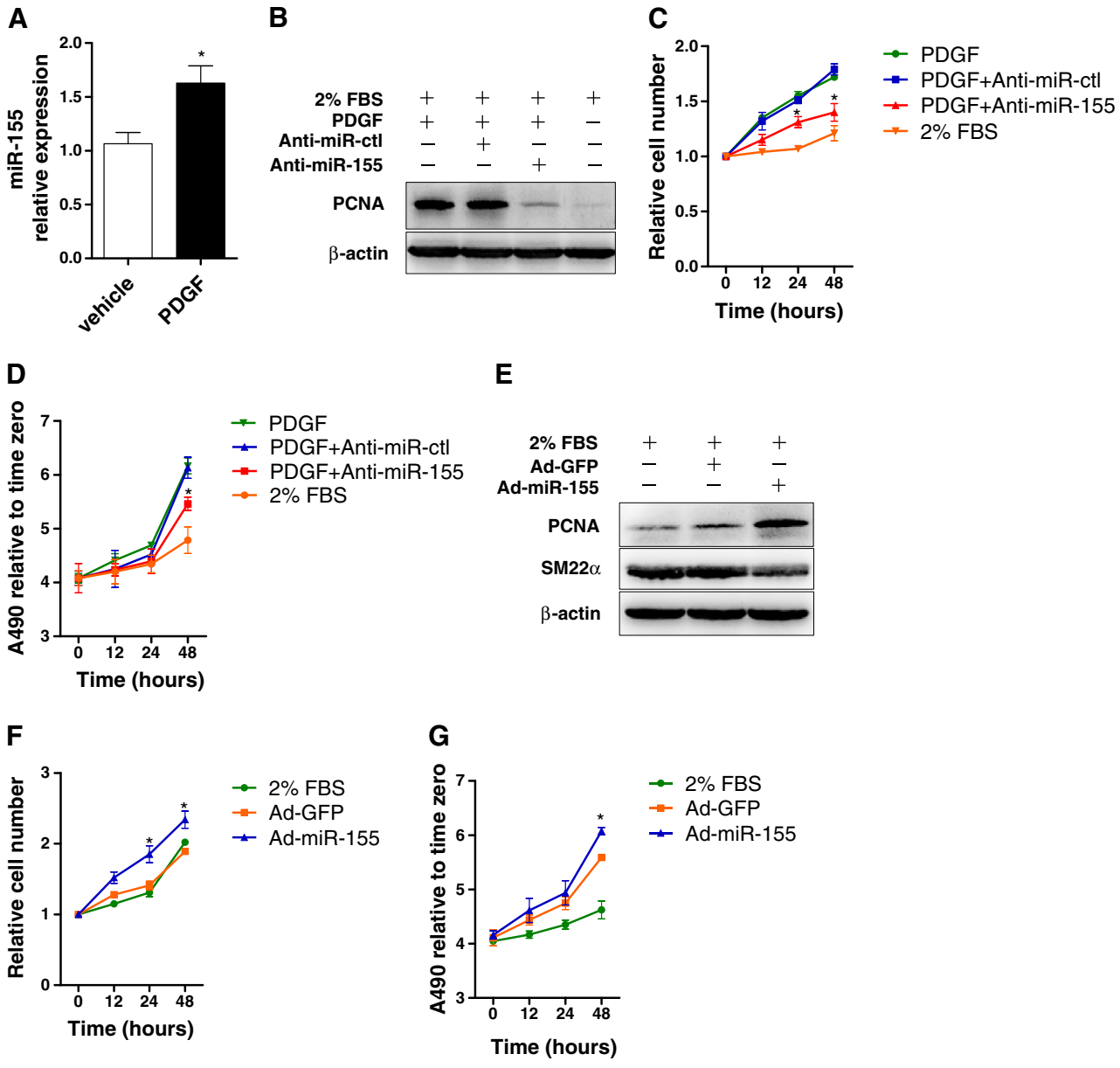

Fig. 2. miR-155 promotes VSMC proliferation *in vitro*. A, VSMCs were serum-starved and treated with PDGF-BB for 12 h, and miR-155 expression was detected by qRT-PCR analysis. *P < 0.05 vs. vehicle control. B, Western blotting for PCNA in VSMCs transfected with anti-miR-155 or anti-miR-ctl and treated with PDGF-BB (10 ng/ml) for 24 h. C, Cell counting of VSMCs transfected with anti-miR-155 (100 nmol/l) or anti-miR-ctl (100 nmol/l) and then treated with PDGF-BB. *P < 0.05 vs. anti-miR-ctl. D, MTS assays using VSMCs transfected with anti-miR-155 or anti-miR-ctl for 12 to 48 h and then exposed to PDGF-BB, as described above. E, Western blotting analysis of PCNA and SM22α expression in VSMCs infected with Ad-miR-155 or Ad-GFP. F, Cell counting of VSMCs infected with Ad-miR-155 or Ad-GFP. *P < 0.05 vs. Ad-GFP. G, MTS assays on VSMCs infected with the indicated vectors and treated as described for panel E. *P < 0.05 vs. Ad-GFP. All experiments were performed in triplicate.

expression of proliferating cell nuclear antigen (PCNA), a proliferation marker (Fig. 2B). Cell-counting and MTS assays yielded similar results, indicating that anti-miR-155 significantly decreased PDGF-BB-induced VSMC proliferation (Fig. 2C, D). In contrast, infection of quiescent VSMCs with Ad-miR-155 but not Ad-GFP significantly reduced the expression of SM22α (a differentiation marker) and increased the expression of PCNA (Fig. 2E). Cell-counting and MTS assays revealed that miR-155 overexpression significantly promoted VSMC proliferation (Fig. 2F, G). Together, these data indicate that miR-155 promotes VSMC proliferation *in vitro*.

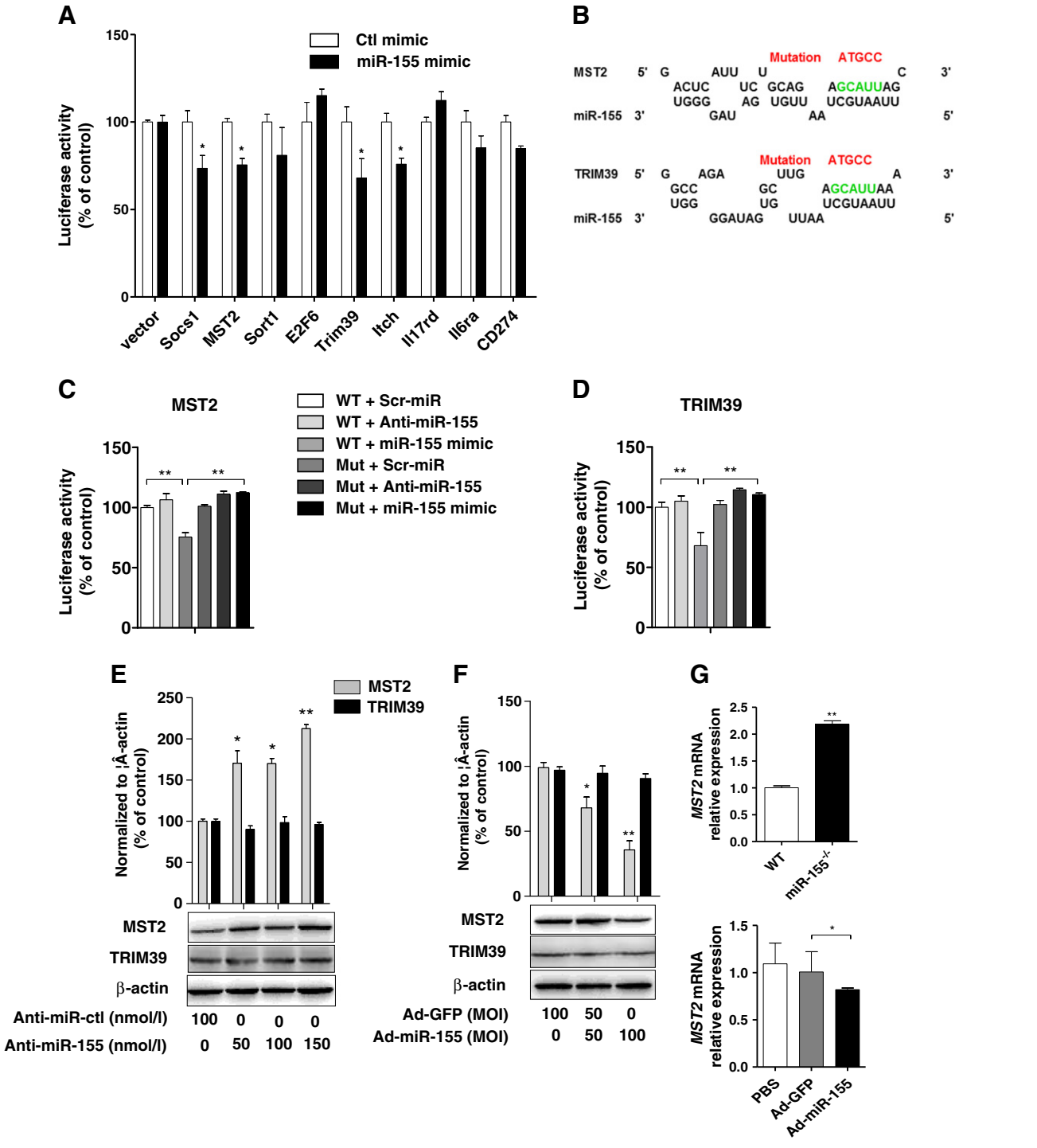

Fig. 3. Identification of miR-155 targets in VSMCs. A, Luciferase reporter assays in HEK293 cells transfected with constructs containing the 3′UTR of potential miR-155 targets in the presence of miR-155 mimics or non-targeting control mimics (ctl mimic). The pmirGLO vector and socs1 were used as negative and positive controls, respectively. B, The miR-155-binding site in the 3′UTR of the mouse MST2 and TRIM39 mRNA (green); the mutated site is shown in red. C and D, Luciferase reporter assays in HEK293 cells transfected with the constructs containing the WT or mutated MST2 3′UTR (C) or the WT or mutated TRIM39 3′UTR (D) after treatment with the miR-155 mimic, anti-miR-155 or control Scr-miR microRNA (anti-miR-ctl). **P < 0.01 vs. WT 3′UTR + anti-miR-155 or vs. WT + miR-155 mimics. E and F, VSMCs were transfected with anti-miR-ctl (100 nmol/l) or anti-miR-155 (50, 100 and 150 nmol/l), and the total protein was harvested from VSMCs (E) or the cells were infected with Ad-GFP (100 MOI) and Ad-miR-155 (50 and 100 MOI) (F) and analyzed by Western blotting against MST2 and TRIM39. *P < 0.05, **P < 0.01 vs. anti-miR-ctl or Ad-GFP. G, qRT-PCR analysis of the MST2 mRNA levels in the injured vessels of WT, miR-155-overexpressing WT, and miR-155$^{-/-}$ mice. Bars represent the means ± SD; n = 6 in each group. *P < 0.05 vs. Ad-GFP; **P < 0.01 vs. WT.

3.3. MST2 is a direct target of miR-155 in VSMCs

To elucidate the mechanism by which miR-155 promotes VSMC proliferation, eight potential targets related to VSMC proliferation or inflammation were tested using luciferase reporter assays; these targets were selected using several miRNA-target prediction algorithms including miRanda [22] and RNAhybrid [23]. Suppressor of cytokine signaling 1 (socs1), a target of miR-155, was used as a positive control, and the empty vector pmirGLO was used as a negative control. Three among the eight reporters were repressed by a miR-155 mimic (Fig. 3A). MST2, a core component of the Hippo signaling pathway, regulates cell proliferation, growth and apoptosis [14], and the E3 ubiquitin-protein ligase TRIM39 has a pro-apoptotic effect by inhibiting APC/C-Cdh1-mediated poly-ubiquitination [26]. Therefore, we mutated the miR-155-binding site resides in the 3′UTR of the MST2 and TRIM39 mRNAs and performed luciferase reporter assays using a miR-155 mimic and a miR-155 inhibitor (Fig. 3B). We observed that in cells containing wild-type (WT) MST2 3′UTR, luciferase activity was reduced by 31% upon treatment with the miR-155 mimic compared with control microRNA ($P < 0.01$); mutation of the miR-155-binding site in the MST2 3′UTR almost completely restored luciferase activity in the presence of the miR-155 mimic. Similar results were obtained with cells containing WT and mutant TRIM39 3′UTR (Fig. 3C, D). To confirm these observations *in vitro*, we transfected VSMCs with anti-miR-155 and anti-miR-ctl and observed that anti-miR-155 increased the MST2 protein level but not the TRIM39 protein level in a dose-dependent manner (Fig. 3E). Conversely, overexpression of miR-155 in VSMCs decreased expression of the MST2 protein but not the TRIM39 protein in a dose-dependent manner (Fig. 3F). We observed consistent results using qRT-PCR to analyze MST2 expression *in vivo*; in wire-injured vessels, MST2 expression was increased in miR-155$^{-/-}$ mice and decreased in WT mice overexpressing miR-155 (Fig. 3G). Together, these data indicate that miR-155 directly targets MST2 in VSMCs via the miR-155-binding site in the MST2 3′UTR.

3.4. Downregulation of MST2 by miR-155 increases VSMC proliferation via the ERK1/2 pathway

To elucidate the cellular and molecular mechanisms by which miR-155 promotes VSMC proliferation, we examined the effect of miR-155 on signaling pathways related to cell proliferation, including PI3K/Akt, ERK1/2, JNK and p38 by performing western blotting using antibodies against the active (phosphorylated) forms of these kinases. As shown in Fig. 4A, overexpression of miR-155 significantly downregulated MST2 expression and increased PI3K/Akt and ERK1/2 phosphorylation in VSMCs but did not affect the phosphorylation of JNK and p38. In contrast, ERK1/2 activation was significantly repressed upon transfection with anti-miR-155 but not anti-miR-ctl; however, there were no

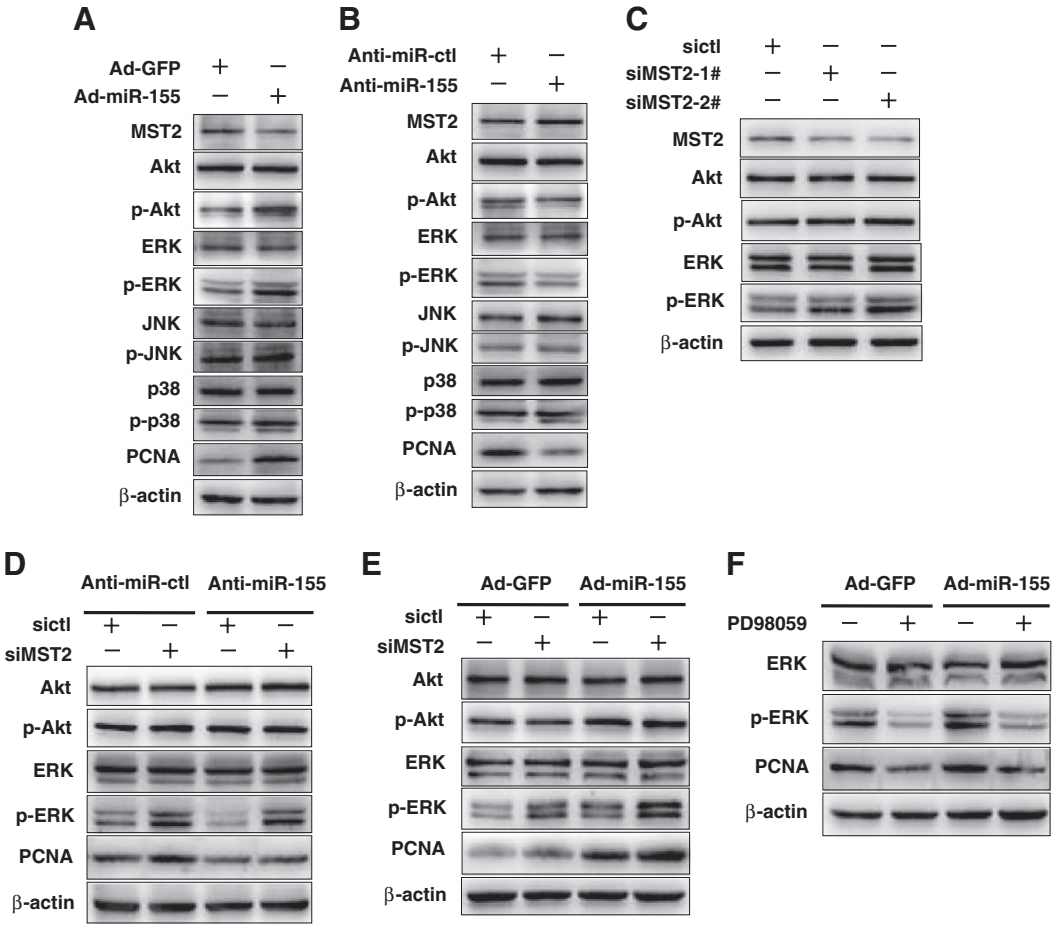

Fig. 4. Role of MST2 in miR-155-mediated VSMC proliferation. A and B, Western blotting analysis for total and phosphorylated Akt, ERK1/2, JNK, p38, and PCNA in VSMCs (A) infected with Ad-GFP or Ad-miR-155 for 24 h; (B) Transfected with anti-miR-ctl or anti-miR-155 for 24 h and then exposed to 10% FCS for 2 h. C, Two different siRNAs against MST2 mRNA (100 nmol/l each) were used to transfect VSMCs for 24 h in 0.1% FCS DMEM. The VSMCs were then incubated with 10% FCS for 2 h, and the total protein lysates were collected and analyzed by Western blotting for total and phosphorylated Akt and ERK1/2. D and E, VSMCs with MST2 knocked down by siMST2 transfection were transfected with anti-miR-155 or anti-miR-ctl (D), or infected with Ad-miR-155 or Ad-GFP (E). The total and phosphorylated Akt and ERK1/2 levels were determined by Western blotting using the respective antibodies. F, VSMCs transfected with Ad-miR-155 or Ad-GFP were treated with or without PD98059. The total and phosphorylated ERK1/2 levels were determined by Western blotting using the respective antibodies. PCNA expression was measured as an indicator of cell proliferation. All experiments were performed in three independent experiments.

significant changes in PI3K/Akt, JNK and p38 phosphorylation (Fig. 4B). These results suggest that additional mechanisms might regulate the activation of PI3K/Akt in VSMCs overexpressing miR-155. To further examine the role of MST2 in miR-155-mediated VSMC proliferation, we designed two different siRNAs to specifically silence MST2 expression. Western blotting analysis revealed that both siRNAs could efficiently knock down MST2 expression compared with control siRNA. Notably, MST2 knockdown also resulted in the activation of ERK1/2 but no significant change in PI3K/Akt phosphorylation (Fig. 4C). Subsequently, we knocked down MST2 and treated VSMCs with miR-155 inhibitor anti-miR-155. Western blotting analysis revealed that knockdown of MST2 in anti-miR-155-transfected cells rescued ERK1/2 but not PI3K/Akt phosphorylation and increased the PCNA protein level (Fig. 4D). Conversely, knockdown of MST2 using a specific siRNA further promoted ERK1/2 phosphorylation induced by miR-155 overexpression (Fig. 4E, lane 4 versus lane 3). The downregulation of MST2 by miR-155 and the ability of MST2 to block activation of ERK1/2 by miR-155 suggest that MST2 is a crucial mediator of miR-155 in regulating ERK1/2 signaling. Furthermore, we observed that pharmacological inhibition of the ERK1/2 pathway by PD98059 abolished miR-155-overexpression-induced upregulation of PCNA (Fig. 4F). In addition, wound-scratch assay showed that overexpression of miR-155 markedly increased the migration of VSMCs. However, the promoting action of miR-155 on VSMC migration could be abolished by overexpressing MST2 (Supplementary Fig. 4). Together, these results suggest that miR-155 regulates VSMC proliferation and migration by targeting MST2 and activating ERK1/2 signaling.

3.5. miR-155-mediated downregulation of MST2 increases NF-κB, p47^{phox}, and HO-1 expression

To further elucidate the role of MST2 in vascular remodeling, immunofluorescent staining was performed on sections of the injured femoral arteries from WT and miR-155$^{-/-}$ mice. We observed that MST2 expression was significantly increased in the injured lesions of miR-155$^{-/-}$ mice compared with WT mice (Fig. 5A). Furthermore, these results were consistent with Western blotting analyses performed on injured arteries from WT and miR-155$^{-/-}$ mice; deletion of miR-155 significantly increased MST2 expression (Fig. 5B). Next, we examined which physiological and pathological processes were involved in miR-155-mediated downregulation of MST2. Using qRT-PCR, we examined the expression of iNOS, HO-1, p47^{phox}, p22^{phox}, NF-κB, TNF-α, and IL-1β in the injured arteries of WT, miR-155$^{-/-}$ and miR-155-overexpressing mice. Notably, the iNOS, HO-1, p47^{phox}, and NF-κB expression levels were significantly reduced in the injured arteries of miR-155$^{-/-}$ mice compared with WT mice. Conversely, the expression of these genes was significantly higher in miR-155-overexpressing mice compared with Ad-GFP-infected mice. However, there was no significant difference in p22^{phox}, TNF-α, and IL-1β expression in the injured arteries of miR-155-overexpressing mice compared with Ad-GFP-infected mice (Fig. 5C–I). Together, these data suggest that miR-155-mediated downregulation of MST2 increases inflammation and oxidative stress, evidenced by upregulation of NF-κB and p47^{phox} expression.

3.6. MST2 mediates miR-155-promoted inflammation and oxidative stress responses through the Raf-1–MEK–ERK1/2 pathway

MST2 is a kinase and the core component of Hippo pathway, which mediates diverse physiological and pathological processes [27–29]. To elucidate the mechanism by which MST2 modulates inflammation and oxidative stress, we downregulated MST2 expression in VSMCs and monitored the expression of inflammation- and oxidative stress-related genes. Notably, downregulation of MST2 caused increased expression of p47^{phox} and NF-κB (Fig. 6A). To examine whether miR-155 was involved in these processes, we tested the effect of miR-155 overexpression and anti-miR-155-mediated functional inhibition of miR-155 activity on the expression and phosphorylation of p47^{phox} and NF-κB using Ad-miR-155- and anti-miR-155-transfected VSMCs. As shown in Fig. 6B, miR-155 overexpression significantly increased phosphorylation of p47^{phox} and NF-κB. By contrast, inhibition of miR-155 by anti-miR-155 reduced phosphorylation of p47^{phox} and NF-κB. These results suggest that miR-155 participates in both inflammatory and oxidative stress responses by downregulating MST2 in VSMCs. To test the hypothesis, we examined the functional roles of MST2 in miR-155-mediated inflammatory and oxidative stress responses. Silencing of MST2 in VSMCs transfected with anti-miR-155 increased the expression and phosphorylation of p47^{phox} and NF-κB compared with control groups (Fig. 6C). Conversely, overexpression of MST2 in Ad-miR-155-infected VSMCs reduced the expression and phosphorylation of p47^{phox} and NF-κB (Fig. 6D). Together, these results indicate that miR-155-dependent regulation of p47^{phox} and NF-κB by MST2 links inflammation and oxidative stress.

To determine which pathway mediates miR-155-induced inflammation and oxidative stress response, MST2 was downregulated in VSMCs, and the cells were incubated with the PI3K/Akt, ERK1/2, NF-κB, and NAD(P)H inhibitors LY294002, PD98059, CAY10576 and APOCYNIN, respectively, for 2 h before exposure to 10% FCS. Notably, inhibition of ERK1/2 blocked siMST2-induced phosphorylation of p47^{phox} and NF-κB (Fig. 6E). To confirm this observation, VSMCs (not transfected with siMST2) were incubated with PD98059, and Western blotting was used to analyze the phosphorylation of p47^{phox} and NF-κB. As shown in Fig. 6F, inhibition of the ERK1/2 pathway also reduced the phosphorylation of p47^{phox} and NF-κB. Interestingly, inhibition of NF-κB by CAY10576 decreased the activation of p47^{phox} in VSMCs transfected with siMST2. Consistent with this observation, inhibition of NAD(P)H using APOCYNIN also reduced the phosphorylation of NF-κB (Fig. 6E). Together, these data indicate that miR-155 mediates the potential link between inflammation and oxidative stress via the ERK1/2 signaling pathway.

Alteration in the MST2–Raf-1 interaction affects the ERK1/2 pathway [17]. Therefore, we examined how miR-155 impinges on MST2-mediated regulation of the ERK1/2 pathway. Coimmunoprecipitation analysis of the lysates from VSMCs infected with Ad-miR-155 revealed a significant increase in MEK levels and decrease of MST2 levels in anti-Raf-1-immunoprecipitates compared with Ad-GFP-infected cells. By contrast, transfection with anti-miR-155 increased MST2 levels and reduced MEK levels in the complexes (Fig. 6G). As expected, miR-155 overexpression also increased phosphorylation of MEK and ERK1/2, whereas transfection with anti-miR-155 reduced their phosphorylation (Fig. 6G). Together, these observations indicate that MST2 competes with MEK to bind Raf-1; furthermore, downregulation of MST2 by miR-155 alters the interaction of MEK with Raf-1 and MST2, leading to activation of ERK1/2 signaling.

4. Discussion

In this study, we observed that in response to vascular injury, miR-155 directly represses MST2 to promote VSMC proliferation and coordinate inflammation and oxidative stress via the Raf-1–MEK–ERK1/2 pathways. The following observations support this conclusion: (1) Neointimal formation in wire-injured arteries was decreased and increased by loss and gain of miR-155, respectively; (2) miR-155 decreased MST2 expression in cultured VSMCs, whereas MST2 expression was elevated in the neointima of miR-155$^{-/-}$ mice; (3) Downregulation of MST2 by miR-155 increased VSMC proliferation via the ERK1/2 pathway; and (4) MST2 mediates miR-155-induced inflammatory and oxidative stress responses through the Raf-1–MEK–ERK1/2 pathway.

Previously, we observed that miR-155 is significantly upregulated during neointimal hyperplasia induced by carotid artery ligation [10]. However, the mechanisms by which miR-155 regulates vascular remodeling are unclear. miR-155 is an onco-miRNA and is overexpressed in a number of human malignancies, and its oncogenic properties are

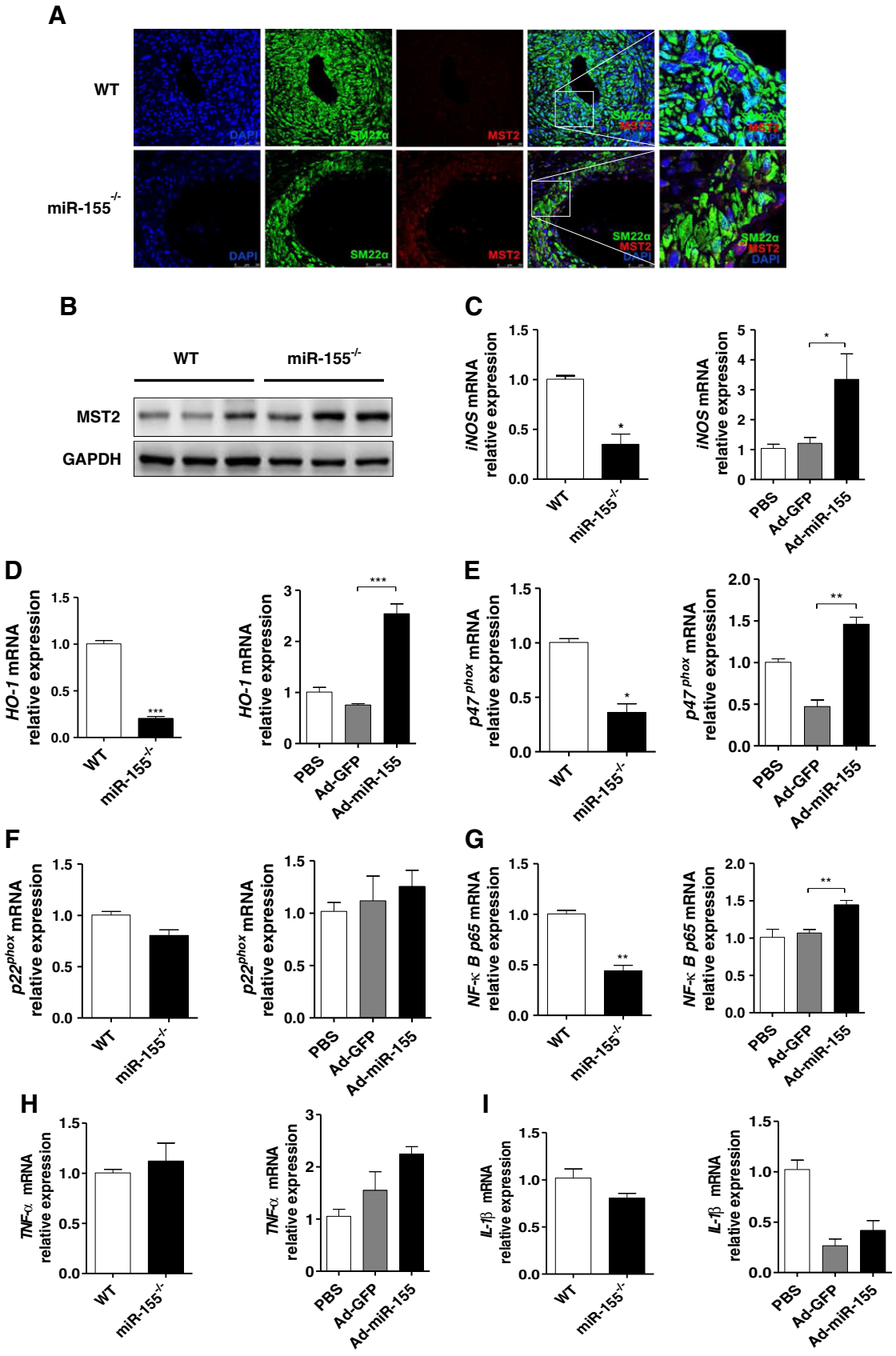

Fig. 5. miR-155-mediated downregulation of MST2 increases expression of NF-κB, $p47^{phox}$, and HO-1. A, Immunofluorescent staining was performed on sections from injured femoral arteries of WT (C57BL/6) and miR-$155^{-/-}$ mice. Red, green and blue staining indicates MST2, SM22α and DAPI, respectively (scale bar, 50 μm). B, Western blotting analysis to measure MST2 expression in injured arteries from WT and miR-$155^{-/-}$ mice (n = 3 in each group). C-I, qRT-PCR analysis of iNOS, HO-1, $p47^{phox}$, $p22^{phox}$, NF-κB, TNF-α and IL1β expression in injured arteries from WT and miR-$155^{-/-}$ mice (*P < 0.05, **P < 0.01, ***P < 0.001 vs. WT) as well as miR-155-overexpressing mice (*P < 0.05, **P < 0.01, ***P < 0.001 vs. Ad-GFP).

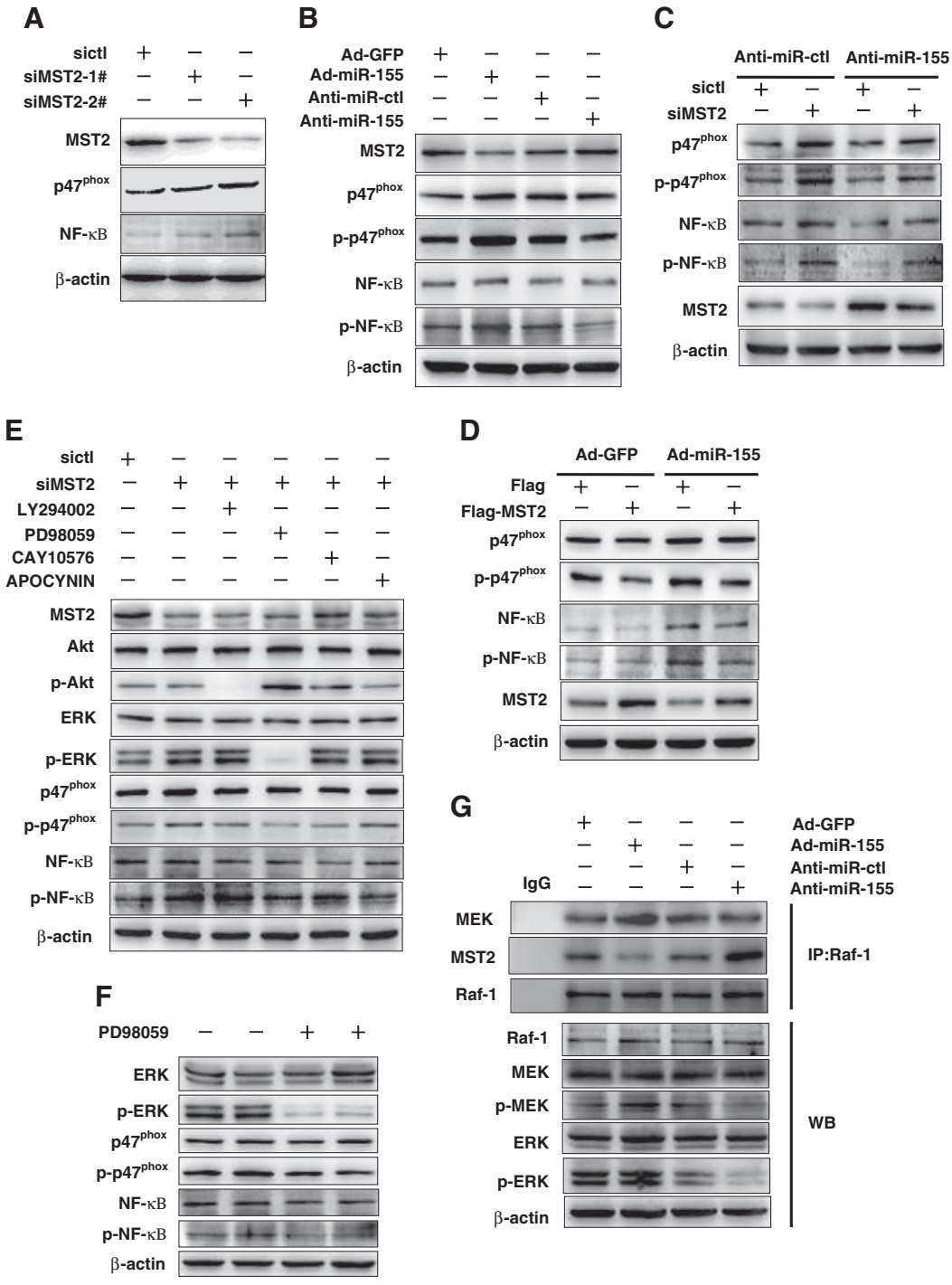

Fig. 6. MST2 mediates miR-155-promoted inflammation and oxidative stress responses through the Raf-1–MEK–ERK1/2 pathway. A, VSMCs were transfected with sictl or siMST2 for 24 h. The total protein lysates were then collected and Western blotting was performed to analyze the expression of MST2, $p47^{phox}$, and NF-κB. B, VSMCs were transfected with Ad-GFP, Ad-miR-155, anti-miR-ctl, or anti-miR-155. After 24 h, expression of the indicated proteins was analyzed by Western blotting. C, VSMCs were transfected with siMST2, anti-miR-ctl, or anti-miR-155; total protein lysates were collected and analyzed by Western blotting to examine the expression of $p47^{phox}$, NF-κB, and their phosphorylated forms. D, VSMCs were transfected with the pCMV-Flag-MST2-MAT plasmid (OE Flag-MST2), the pCMV-Flag- MAT plasmid (Flag), Ad-GFP, or Ad-miR-155; total protein lysates were collected and analyzed by Western blotting to examine the expression of $p47^{phox}$, NF-κB, and their phosphorylated forms. E, VSMCs were transfected with siMST2 or sictl and then treated with the indicated inhibitors. Total protein lysates were collected, and the expression of Akt, ERK, $p47^{phox}$, and NF-κB and their phosphorylated forms was examined by Western blotting. F, VSMCs were treated with or without the ERK inhibitor PD98059. Total protein lysates were collected, and the expression of ERK, $p47^{phox}$, and NF-κB and their phosphorylated forms was analyzed by Western blotting. G, VSMCs were transfected with Ad-GFP, Ad-miR-155, anti-miR-ctl, or anti-miR-155. Anti-Raf-1 immunoprecipitates were analyzed by Western blotting to examine changes in MST2, MEK and Raf-1 levels. All experiments were performed in triplicate.

attributed to stimulation of cellular proliferation, inhibition of caspase-3 activity, and targeting of pro-apoptotic molecules such as TP53BP1 [30–32]. In our study, TUNEL staining and caspase cleavage assay showed that miR-155 overexpression significantly inhibited VSMC apoptosis and the activation of caspase-3 induced by H_2O_2 (Supplementary Fig. 5A, B). Furthermore, Eμ-mmu-miR-155 transgenic mice develop B-cell malignancies [33]. These observations suggest that miR-155 has a proliferative effect. In this study, we used gain- and loss-of-function approaches and observed that miR-155 promoted VSMC proliferation *in vivo* and *in vitro* in response to vascular injury.

This study identified that MST2 is significantly upregulated in injured arteries of miR-155$^{-/-}$ mice and is negatively regulated by miR-155 in cultured VSMCs; luciferase reporter assays and Western blotting analyses revealed that MST2 is a novel target of miR-155. By targeting MST2, miR-155 promotes VSMC proliferation in response to vascular injury. Genetic screens in *Drosophila* have shown that loss of function of MST2 and its close homologue MST1 resulted in overgrown tissues containing a greater number of normal-sized cells. These mutant cells expressed elevated levels of cyclin E and underwent increased cell growth and proliferation as well as impaired apoptosis [34]. Consistent with this study, in mammals, deletion of both MST2 and MST1 in hepatocytes resulted in significantly enlarged livers due to excessive proliferation [35]. Furthermore, silencing of MST2 in mouse or human Raf-1$^{-/-}$ cells causes reduced sensitivity to apoptosis, whereas overexpression of MST2 induces apoptosis [15]. These observations suggest that MST2 has an important role in regulating proliferation and apoptosis.

ERK1/2 is activated in various animal models after vascular injury, and VSMC proliferation and vascular remodeling in balloon-injured arteries are attenuated by both ERK1/2 inhibitor and gene transfer of the ERK1/2 dominant-negative mutant [36–38]. We previously showed that overexpression of SM22α significantly inhibited the Ras–Raf–MEK–ERK1/2 signaling cascade and reduced mitogen-stimulated proliferation of VSMCs and injury-induced neointimal remodeling [39]. MST2 is a member of the germinal center kinase group II (GCK II) family of mitogen-activated protein kinase (MAPK)-related kinases [13,40]. The MAPK pathway can be regulated by the overall strength and duration of the ERK signal [13]. Proteomic analysis of Raf-1 signaling complexes revealed that Raf-1 interacted with MST2 [15], which enables Raf-1, MST2 and MEK to signal the MAP kinases. MST2 binds Raf-1 at two distinct sites that overlap with the MEK-binding domains [16], suggesting that MST2 competes with MEK to bind Raf-1 under certain conditions, thus affecting MAPK signaling. Consistent with this observation, when a disruptor peptide, i.e., stearoylated-MST2 was used to dissociate MST2 from Raf-1, binding of MEK to Raf-1 as well as activation of MEK and ERK1/2 was significantly increased [17]. We observed that miR-155 activates the ERK1/2 pathway by directly repressing the expression of MST2, consequently enhancing the interaction of between Raf-1 and MEK and promoting VSMC proliferation as well as injury-induced neointimal hyperplasia.

As the chief effector cell in vascular injury, VSMCs coordinate and synchronize extremely complex inflammatory, proliferative, differentiation and oxidative stress programs [1–3]. miR-155 is a typical multifunctional microRNA with distinct expression profiles and plays a critical role in various physiological and pathological processes such as inflammation, proliferation, differentiation and oxidative stress [2,3]. miR-155 plays a critical role in the development of atherosclerosis; here, vascular inflammation is sustained and amplified by repression of BCL6-mediated inhibition of CCL2 expression [41]. Similarly, in atherosclerotic lesions, miR-155 increased Nos2 expression in pro-inflammatory macrophages by upregulating miR-342-5p-mediated repression of Akt1 [42]. Interestingly, miR-155 expression in macrophages, but not cardiomyocytes, promoted cardiac inflammation and hypertrophy [41], while another report showed that miR-155 induced pathological cardiomyocyte hypertrophy in pressure overload-induced hypertrophic hearts [43]. These data suggest that the deficit of miR-155 facilitates protection from atherosclerosis and cardiac hypertrophy. Conversely, some evidences have indicated that miR-155 modulated angiotensin signaling in cardiovascular system. The angiotensin II type 1 receptor (AT1R) expression was positively correlated with blood pressure and negatively correlated with miR-155 expression level [44]. Loss of miR-155-mediated depression of AT1R could be implicated in hypertension and cardiovascular diseases [12]. However, our data showed that there were no statistically significant differences between WT and miR-155$^{-/-}$ mice in blood pressure (Supplementary Fig. 6). So, miR-155-mediated vascular remodeling might be independent from blood pressure under physiological condition.

It is not known whether miR-155 upregulation is correlated with NF-κB activation. Although miR-155 expression and NF-κB activation significantly elevated at early stages of hepatocarcinogenesis in a mouse model [45], our observations reveal that miR-155 activates NF-κB inflammatory pathways by downregulating MST2 via the ERK1/2 pathway. It is well established that TNF-α and IL-1β are major inflammatory factors. However, our result showed that overexpression of miR-155 at wire-injured femoral artery did not affect TNF-α and IL-1β mRNA levels. As a result, we performed an ELISA assay to determine whether overexpression of miR-155 affected the protein levels of TNF-α and IL-1β. As shown in Supplementary Fig. 7, overexpression of miR-155 upregulated TNF-α expression but did not change IL-1β level

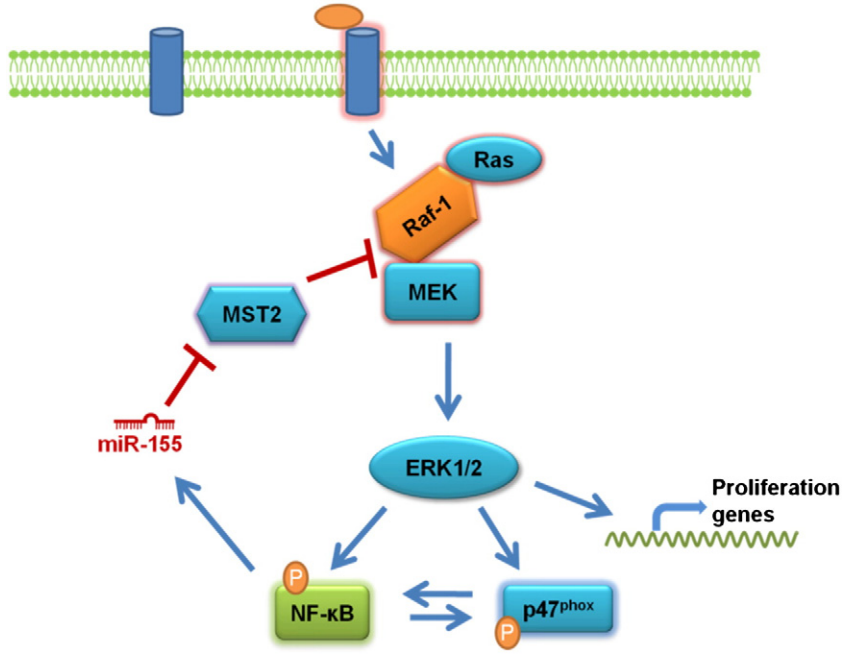

Fig. 7. Proposed model for miR-155-mediated crosstalk between inflammation and oxidative stress. miR-155 targets and downregulates MST2, which competes with MEK for binding to Raf-1 (MST2–Raf-1 accumulates at the expense of MEK–Raf-1), and activates ERK1/2 pathway, subsequently leading to the activation of NF-κB and p47^{phox}.

in tissue lysates. Consistent with our findings, Zhang et al. recently reported that overexpression of miR-155 markedly increased TNF-α but did not affect IL-1β level both in the ligated vessels and cultured BMMs [10]. These data imply that additional mechanisms might be involved in regulating the expression of IL-1β in the injured vessels.

Oxidative stress and inflammation are frequently involved in cardiovascular diseases simultaneously; these processes are a common feature at early stages of atherosclerosis in response to vascular injury [46,47]. $p47^{phox}$ is an essential component of NAD(P)H oxidase, which is the critical source of ROS in atherosclerotic lesions [48]. However, reduced phosphorylation of SM22α abolishes Ang-II-induced ROS production via the activated PKCδ-$p47^{phox}$ axis and inhibits VSMC hypertrophy and hyperplasia *in vitro* and *in vivo*. Consistent with $p47^{phox}$-mediated oxidative stress in VSMCs, we observed that miR-155 elevates the total $p47^{phox}$ level and increased its phosphorylation; the latter effect is mediated by MST2 via the ERK1/2 pathway [49]. Activated NF-κB and oxidative stress are closely associated with many risk factors for atherosclerosis including vessel injury [46]. Notably, we observed that the NF-κB inhibitor CAY10576 inhibited MST2-mediated ERK1/2 activation and $p47^{phox}$-mediated oxidative stress; however, the NAD(P)H oxidase inhibitor APOCYNIN reduced phosphorylation of NF-κB. These data suggest that the inflammatory and oxidative stress pathways are coordinated by miR-155-mediated regulation of MST2 via Raf-1–MEK–ERK1/2 signaling.

In summary, we identified that miR-155 promotes VSMC proliferation; this effect is partially mediated by repression of MST2, which alters the interaction of Raf-1 with MST2 and MEK, leading to activation of ERK1/2. Activation of ERK1/2 couples oxidative stress with inflammatory pathways and further increases miR-155 expression (Supplementary Fig. 8); Interestingly, overexpression of miR-155 in the injured arterial wall also enhanced PDGF expression (Supplementary Fig. 9). Totally, a positive feedback loop is established to promote VSMC proliferation (Fig. 7). Our *in vivo* and *in vitro* observations indicate that miR-155 is an important mediator of neointimal hyperplasia and that inhibition of endogenous miR-155 might be a novel therapeutic strategy in vascular injury and remodeling.

Conflict of interest statement

No potential conflicts of interest were disclosed.

Transparency document

The Transparency document associated with this article can be found, in the online version.

Acknowledgements and funding

Zhang Y, He M, Zhang XH, Zhang RN, Ma D, and Wu XL carried out the experiments. Zheng B and Wen JK reviewed the data and helped in the design and preparation of the manuscript. This study was supported by the National Natural Science Foundation of China (Nos. 31271396, 31271224, 31301136) and the National Basic Research Program of China (No. 2012CB518601).

Appendix A. Supplementary data

Supplementary data to this article can be found online at http://dx.doi.org/10.1016/j.bbadis.2015.04.012.

References

[1] B. Zheng, M. Han, J.K. Wen, Role of Kruppel-like factor 4 in phenotypic switching and proliferation of vascular smooth muscle cells, IUBMB Life 62 (2010) 132–139.
[2] K.K. Koh, P.C. Oh, M.J. Quon, Does reversal of oxidative stress and inflammation provide vascular protection? Cardiovasc. Res. 81 (2009) 649–659.
[3] M.V. Autieri, Kruppel-like factor 4: transcriptional regulator of proliferation, or inflammation, or differentiation, or all three? Circ. Res. 102 (2008) 1455–1457.
[4] R.A. McDonald, A. Hata, M.R. MacLean, N.W. Morrell, A.H. Baker, MicroRNA and vascular remodelling in acute vascular injury and pulmonary vascular remodelling, Cardiovasc. Res. 93 (2012) 594–604.
[5] C. Urbich, A. Kuehbacher, S. Dimmeler, Role of microRNAs in vascular diseases, inflammation, and angiogenesis, Cardiovasc. Res. 79 (2008) 581–588.
[6] D. Torella, C. Iaconetti, D. Catalucci, G.M. Ellison, A. Leone, C.D. Waring, A. Bochicchio, C. Vicinanza, I. Aquila, A. Curcio, G. Condorelli, C. Indolfi, MicroRNA-133 controls vascular smooth muscle cell phenotypic switch in vitro and vascular remodeling in vivo, Circ. Res. 109 (2011) 880–893.
[7] X. Liu, Y. Cheng, S. Zhang, Y. Lin, J. Yang, C. Zhang, A necessary role of miR-221 and miR-222 in vascular smooth muscle cell proliferation and neointimal hyperplasia, Circ. Res. 104 (2009) 476–487.
[8] A.Y. Rangrez, Z.A. Massy, V. Metzinger-Le Meuth, L. Metzinger, miR-143 and miR-145: molecular keys to switch the phenotype of vascular smooth muscle cells, Circ. Cardiovasc. Genet. 4 (2011) 197–205.
[9] T.A. Harris, M. Yamakuchi, M. Ferlito, J.T. Mendell, C.J. Lowenstein, MicroRNA-126 regulates endothelial expression of vascular cell adhesion molecule 1, Proc. Natl. Acad. Sci. U. S. A. 105 (2008) 1516–1521.
[10] R.N. Zhang, B. Zheng, L.M. Li, J. Zhang, X.H. Zhang, J.K. Wen, Tongxinluo inhibits vascular inflammation and neointimal hyperplasia through blockade of the positive feedback loop between miR-155 and TNF-alpha, Am. J. Physiol. Heart Circ. Physiol. 307 (2014) H552–H562.
[11] F.J. Tian, L.N. An, G.K. Wang, J.Q. Zhu, Q. Li, Y.Y. Zhang, A. Zeng, J. Zou, R.F. Zhu, X.S. Han, N. Shen, H.T. Yang, X.X. Zhao, S. Huang, Y.W. Qin, Q. Jing, Elevated microRNA-155 promotes foam cell formation by targeting HBP1 in atherogenesis, Cardiovasc. Res. 103 (2014) 100–110.
[12] I. Faraoni, F.R. Antonetti, J. Cardone, E. Bonmassar, miR-155 gene: a typical multifunctional microRNA, Biochim. Biophys. Acta 1792 (2009) 497–505.
[13] E.E. O'Neill, D. Matallanas, W. Kolch, Mammalian sterile 20-like kinases in tumor suppression: an emerging pathway, Cancer Res. 65 (2005) 5485–5487.
[14] J. Avruch, D. Zhou, J. Fitamant, N. Bardeesy, F. Mou, L.R. Barrufet, Protein kinases of the Hippo pathway: regulation and substrates, Semin. Cell Dev. Biol. 23 (2012) 770–784.
[15] E. O'Neill, L. Rushworth, M. Baccarini, W. Kolch, Role of the kinase MST2 in suppression of apoptosis by the proto-oncogene product Raf-1, Science 306 (2004) 2267–2270.
[16] D. Matallanas, M. Birtwistle, D. Romano, A. Zebisch, J. Rauch, A. von Kriegsheim, W. Kolch, Raf family kinases: old dogs have learned new tricks, Genes Cancer 2 (2011) 232–260.
[17] D. Romano, L.K. Nguyen, D. Matallanas, M. Halasz, C. Doherty, B.N. Kholodenko, W. Kolch, Protein interaction switches coordinate Raf-1 and MST2/Hippo signalling, Nat. Cell Biol. 16 (2014) 673–684.
[18] M. Wang, K. Ihida-Stansbury, D. Kothapalli, M.C. Tamby, Z. Yu, L. Chen, G. Grant, Y. Cheng, J.A. Lawson, R.K. Assoian, P.L. Jones, G.A. Fitzgerald, Microsomal prostaglandin e2 synthase-1 modulates the response to vascular injury, Circulation 123 (2011) 631–639.
[19] C. Wang, M. Han, X.M. Zhao, J.K. Wen, Kruppel-like factor 4 is required for the expression of vascular smooth muscle cell differentiation marker genes induced by all-trans retinoic acid, J. Biochem. 144 (2008) 313–321.
[20] K.H. Chen, X. Guo, D. Ma, Y. Guo, Q. Li, D. Yang, P. Li, X. Qiu, S. Wen, R.P. Xiao, J. Tang, Dysregulation of HSG triggers vascular proliferative disorders, Nat. Cell Biol. 6 (2004) 872–883.
[21] S.L. Straszewski-Chavez, I.P. Visintin, N. Karassina, G. Los, P. Liston, R. Halaban, A. Fadiel, G. Mor, XAF1 mediates tumor necrosis factor-alpha-induced apoptosis and X-linked inhibitor of apoptosis cleavage by acting through the mitochondrial pathway, J. Biol. Chem. 282 (2007) 13059–13072.
[22] B.P. Lewis, C.B. Burge, D.P. Bartel, Conserved seed pairing, often flanked by adenosines, indicates that thousands of human genes are microRNA targets, Cell 120 (2005) 15–20.
[23] M. Rehmsmeier, P. Steffen, M. Hochsmann, R. Giegerich, Fast and effective prediction of microRNA/target duplexes, RNA 10 (2004) 1507–1517.
[24] B. Zheng, M. Han, Y.N. Shu, Y.J. Li, S.B. Miao, X.H. Zhang, H.J. Shi, T. Zhang, J.K. Wen, HDAC2 phosphorylation-dependent Klf5 deacetylation and RARalpha acetylation induced by RAR agonist switch the transcription regulatory programs of p21 in VSMCs, Cell Res. 21 (2011) 1487–1508.
[25] A. Talasila, H. Yu, M. Ackers-Johnson, M. Bot, T. van Berkel, M.R. Bennett, I. Bot, S. Sinha, Myocardin regulates vascular response to injury through miR-24/-29a and platelet-derived growth factor receptor-beta, Arterioscler. Thromb. Vasc. Biol. 33 (2013) 2355–2365.
[26] N.J. Huang, L. Zhang, W. Tang, C. Chen, C.S. Yang, S. Kornbluth, The Trim39 ubiquitin ligase inhibits APC/CCdh1-mediated degradation of the Bax activator MOAP-1, J. Cell Biol. 197 (2012) 361–367.
[27] B.A. Callus, A.M. Verhagen, D.L. Vaux, Association of mammalian sterile twenty kinases, Mst1 and Mst2, with hSalvador via C-terminal coiled-coil domains, leads to its stabilization and phosphorylation, FEBS J. 273 (2006) 4264–4276.
[28] J. Cai, N. Zhang, Y. Zheng, R.F. de Wilde, A. Maitra, D. Pan, The Hippo signaling pathway restricts the oncogenic potential of an intestinal regeneration program, Genes Dev. 24 (2010) 2383–2388.
[29] J.C. Boggiano, P.J. Vanderzalm, R.G. Fehon, Tao-1 phosphorylates Hippo/MST kinases to regulate the Hippo–Salvador–Warts tumor suppressor pathway, Dev. Cell 21 (2011) 888–895.
[30] S. Mattiske, R.J. Suetani, P.M. Neilsen, D.F. Callen, The oncogenic role of miR-155 in breast cancer, Cancer epidemiology, biomarkers & prevention: a publication of the American Association for Cancer Research, cosponsored by the American Society of Preventive Oncology, 21 2012, pp. 1236–1243.

[31] D. Ovcharenko, K. Kelnar, C. Johnson, N. Leng, D. Brown, Genome-scale microRNA and small interfering RNA screens identify small RNA modulators of TRAIL-induced apoptosis pathway, Cancer Res. 67 (2007) 10782–10788.
[32] E. Tili, C.M. Croce, J.J. Michaille, miR-155: on the crosstalk between inflammation and cancer, Int. Rev. Immunol. 28 (2009) 264–284.
[33] S. Costinean, N. Zanesi, Y. Pekarsky, E. Tili, S. Volinia, N. Heerema, C.M. Croce, Pre-B cell proliferation and lymphoblastic leukemia/high-grade lymphoma in E(mu)-miR155 transgenic mice, Proc. Natl. Acad. Sci. U. S. A. 103 (2006) 7024–7029.
[34] J. Jia, W. Zhang, B. Wang, R. Trinko, J. Jiang, The Drosophila Ste20 family kinase dMST functions as a tumor suppressor by restricting cell proliferation and promoting apoptosis, Genes Dev. 17 (2003) 2514–2519.
[35] L. Lu, Y. Li, S.M. Kim, W. Bossuyt, P. Liu, Q. Qiu, Y. Wang, G. Halder, M.J. Finegold, J.S. Lee, R.L. Johnson, Hippo signaling is a potent in vivo growth and tumor suppressor pathway in the mammalian liver, Proc. Natl. Acad. Sci. U. S. A. 107 (2010) 1437–1442.
[36] Y. Izumi, S. Kim, M. Namba, H. Yasumoto, H. Miyazaki, M. Hoshiga, Y. Kaneda, R. Morishita, Y. Zhan, H. Iwao, Gene transfer of dominant-negative mutants of extracellular signal-regulated kinase and c-Jun NH2-terminal kinase prevents neointimal formation in balloon-injured rat artery, Circ. Res. 88 (2001) 1120–1126.
[37] K. Lai, H. Wang, W.S. Lee, M.K. Jain, M.E. Lee, E. Haber, Mitogen-activated protein kinase phosphatase-1 in rat arterial smooth muscle cell proliferation, J. Clin. Invest. 98 (1996) 1560–1567.
[38] J.M. Pyles, K.L. March, M. Franklin, K. Mehdi, R.L. Wilensky, L.P. Adam, Activation of MAP kinase in vivo follows balloon overstretch injury of porcine coronary and carotid arteries, Circ. Res. 81 (1997) 904–910.
[39] L.H. Dong, J.K. Wen, G. Liu, M.A. McNutt, S.B. Miao, R. Gao, B. Zheng, H. Zhang, M. Han, Blockade of the Ras-extracellular signal-regulated kinase 1/2 pathway is involved in smooth muscle 22 alpha-mediated suppression of vascular smooth muscle cell proliferation and neointima hyperplasia, Arterioscler. Thromb. Vasc. Biol. 30 (2010) 683–691.
[40] I. Dan, N.M. Watanabe, A. Kusumi, The Ste20 group kinases as regulators of MAP kinase cascades, Trends Cell Biol. 11 (2001) 220–230.
[41] S. Heymans, M.F. Corsten, W. Verhesen, P. Carai, R.E. van Leeuwen, K. Custers, T. Peters, M. Hazebroek, L. Stoger, E. Wijnands, B.J. Janssen, E.E. Creemers, Y.M. Pinto, D. Grimm, N. Schurmann, E. Vigorito, T. Thum, F. Stassen, X. Yin, M. Mayr, L.J. de Windt, E. Lutgens, K. Wouters, M.P. de Winther, S. Zacchigna, M. Giacca, M. van Bilsen, A.P. Papageorgiou, B. Schroen, Macrophage microRNA-155 promotes cardiac hypertrophy and failure, Circulation 128 (2013) 1420–1432.
[42] Y. Wei, M. Nazari-Jahantigh, L. Chan, M. Zhu, K. Heyll, J. Corbalan-Campos, P. Hartmann, A. Thiemann, C. Weber, A. Schober, The microRNA-342-5p fosters inflammatory macrophage activation through an Akt1- and microRNA-155-dependent pathway during atherosclerosis, Circulation 127 (2013) 1609–1619.
[43] H.Y. Seok, J. Chen, M. Kataoka, Z.P. Huang, J. Ding, J. Yan, X. Hu, D.Z. Wang, Loss of MicroRNA-155 protects the heart from pathological cardiac hypertrophy, Circ. Res. 114 (2014) 1585–1595.
[44] G. Ceolotto, I. Papparella, A. Bortoluzzi, G. Strapazzon, F. Ragazzo, P. Bratti, A.S. Fabricio, E. Squarcina, M. Gion, P. Palatini, A. Semplicini, Interplay between miR-155, AT1R A1166C polymorphism, and AT1R expression in young untreated hypertensives, Am. J. Hypertens. 24 (2011) 241–246.
[45] B. Wang, S. Majumder, G. Nuovo, H. Kutay, S. Volinia, T. Patel, T.D. Schmittgen, C. Croce, K. Ghoshal, S.T. Jacob, Role of microRNA-155 at early stages of hepatocarcinogenesis induced by choline-deficient and amino acid-defined diet in C57BL/6 mice, Hepatology 50 (2009) 1152–1161.
[46] F.J. Pashkow, D.G. Watumull, C.L. Campbell, Astaxanthin: a novel potential treatment for oxidative stress and inflammation in cardiovascular disease, Am. J. Cardiol. 101 (2008) 58D–68D.
[47] E. Schleicher, U. Friess, Oxidative stress, AGE, and atherosclerosis, Kidney Int. Suppl. (2007) S17–S26.
[48] K. Kinkade, J. Streeter, F.J. Miller, Inhibition of NADPH oxidase by apocynin attenuates progression of atherosclerosis, Int. J. Mol. Sci. 14 (2013) 17017–17028.
[49] P. Lv, S.B. Miao, Y.N. Shu, L.H. Dong, G. Liu, X.L. Xie, M. Gao, Y.C. Wang, Y.J. Yin, X.J. Wang, M. Han, Phosphorylation of smooth muscle 22alpha facilitates angiotensin II-induced ROS production via activation of the PKCdelta–P47phox axis through release of PKCdelta and actin dynamics and is associated with hypertrophy and hyperplasia of vascular smooth muscle cells in vitro and in vivo, Circ. Res. 111 (2012) 697–707.